Characteristics of holey fibers fabricated at different drawing speeds

Faramarz E. Seraji[1], Mahnaz Rashidi[2], and Maryam Karimi[3]

[1]*Optical Communication Group, Iran Telecom Research Center, Tehran, Iran*

[2]*Physics Group, Guilan University, Rasht, Iran*

[3]*Physics Group, Razi University, Kermanshah, Iran*

Received October 10, 2006

The effects of high drawing speeds on parameters of holey fibers are presented. A holey fiber preform structure was made by using tube-in-tube method and was drawn at high speeds with an aim of mass production to meet the demand of next generation communication systems. Transmission parameters such as numerical aperture and normalized frequency of the fabricated holey fibers have been measured and compared with theoretical values based on effective index method. Although the fabricated holey fibers were not of high quality, the analyses of the parameters have shown promising outlook for fabrication of such fibers.

OCIS codes: 060.2310, 060.2330, 060.2280, 060.2270.

During past decade, a new optical fiber called as holey optical fiber (HOF), for its unique properties, is introduced as a candidate for transmission medium for next generation networks[1]. The HOF is normally made from a single material such as silica with an array of air holes running along the length of the fiber cladding. The holes are normally spaced in a periodic arrangement which may not be always needed[2] and they may be arranged randomly. In either case, a HOF can guide light through total internal refraction since the effective refractive index (ERI) of the cladding is lower than that of the core. Therefore, the light guidance arises from average index effect and it does not rely on periodicity of the holes in cladding[3] that can be modeled by approximate[4] and exact methods[5]. The HOFs with different hole configurations have been reported recently[6,7].

In this paper, the effects of drawing speeds on parameters of HOFs are investigated. And the feasibility of manufacturing HOF with a large production scale as that of conventional communication fibers is discussed. In our fabrication approach, we have used tube-in-tube method which is normally used by others[8]. Recently, other method has also been reported[9].

In our measurement attempts, we have evaluated the effective normalized frequency and numerical apertures (NAs) of our fabricated HOFs. The obtained experimental results have been compared with theoretical analyses based on ERI method, which have shown a relatively good agreement. We have also shown the effect of adjacent hole spacing Λ on numerical aperture with a given air filling fraction (d/Λ), where d is hole diameter.

By ERI method, we determine the effective index of the cladding region and then treat it similar to conventional step index fibers for obtaining different parameter values. To obtain the effective index of the cladding region, we solve Maxwell's equations by applying boundary conditions, based on function continuity and its derivative between air-holes and the silica, which results in[10,11]

$$\psi = \begin{cases} AI_0(WR) & \text{(air hole)} \\ BJ_0(RU) + CY_0(RU) & \text{(silica region)} \end{cases}, \quad (1)$$

where $R = r/a$, r is cylindrical parameter of the fiber, a is the air hole radius, and Y_0, J_0, I_0 are Bessel functions. By applying the boundary conditions, we obtain

$$AI_0(W) = BJ_0(U) + CY_0(U),$$

$$B = \frac{A}{J_0(U)}\left[I_0(W) - \frac{C}{A}Y_0(U)\right], \quad (2)$$

where U and W are given as

$$U = k_0 a\sqrt{n_{\rm s}^2 - n_{\rm cl}^2}, \quad W = k_0 a\sqrt{n_{\rm cl}^2 - n_{\rm a}^2}, \quad (3)$$

where $n_{\rm cl}$, $n_{\rm s}$ and $n_{\rm a}$ are refractive indices of cladding, silica material of cladding, and air hole respectively, $k_0 = 2\pi/\lambda$ (λ is the wavelength).

By applying boundary conditions, the A, B, and C constants are determined by using Bessel functions I_0, I_1, J_0, J_1, Y_0, and Y_1 as

$$AWI_1(W) = -\frac{A}{J_0(U)}\left[I_0(W) - \frac{C}{A}Y_0(U)\right] - CUY_1(U),$$

$$C = \frac{A\left[WI_1(W)J_0(U) + UJ_1(U)I_0(W)\right]}{U\left[J_1(U)Y_0(U) - J_0(U)Y_1(U)\right]}, \quad (4)$$

$$B = \frac{A}{J_0(U)} \times \left[I_0(W) - \frac{Y_0(U)\left[WI_1(W)J_0(U) + UJ_1(U)I_0(W)\right]}{U\left[J_1(U)Y_0(U) - J_0(U)Y_1(U)\right]}\right]. \quad (5)$$

NA and effective normalized frequency $V_{\rm eff}$ are obtained as

$$\mathrm{NA} = \sqrt{n_{\rm co}^2 - n_{\rm cl}^2}, \quad V_{\rm eff} = k_0\rho\sqrt{n_{\rm s}^2 - n_{\rm cl}^2}, \quad (6)$$

where $\rho = 0.64\Lambda$ is assumed as effective radius of the HOF, and $n_{\rm co}$ is the refractive index of the core region.

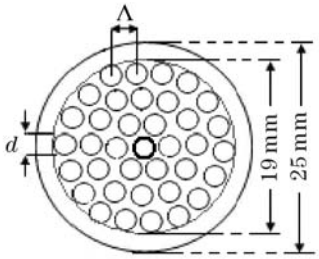

Fig. 1. Cross section of an ideal holey fiber.

Let us consider an ideal holey fiber with a cross section shown schematically in Fig. 1. The simplest procedure to fabricate such a fiber is to make a preform by putting a selected number of capillary tubes side by side stacked in different layers in a holding glass tube around a central capillary tube acting as the core. On drawing this preform, the stacked capillary tubes are converted into air holes in the cladding[12].

Based on Fig. 1, a preform was made by stacking together three layers of 6, 12, and 18 capillary tubes of 1.5-mm inner diameter and 2-mm outer diameter around the core, respectively. The packed set of capillary tubes was inserted in a holding silica tube of 19-mm inner and 25-mm outer diameters, and then the whole set was collapsed to enhance the grip of the tubes together. The average diameter of the fabricated perform was 23.3 mm[12].

One of the effective parameters of a HOF, that ultimately controls its properties, is the air filling fraction in the preform defined as the ratio of air-filled area to the silica-filled area of the preform cross section. With a simple and lengthy calculation, the air filling fraction of the prepared preform was found to be about 63 $mm^2/257$ $mm^2 \approx 0.25$, which was predicted to be about 0.23 after collapsing the preform. This ratio is equivalent to d/Λ. In the calculations, the interstitial air spacing among air holes across the cross section is considered negligible.

Three sections of the preform was drawn by a conventional fiber drawing tower with different speeds of v = 100, 120, and 150 m/min, producing fibers No. 1 to 3, respectively. In the beginning of drawing process, the temperature was set to 1910 °C and was lowered gradually to within 1850 to 1870 °C during the drawing process.

The micrographs of cross-sections of drawn fibers from the preform are shown in Fig. 2. It is shown that the holes have appeared in the cladding not quite in order. The reason of disordered distribution of holes is attributed to high speed drawing of the preform. The holes in first layer adjacent to the core are almost emerged together.

There are also some extended cracks across the fiber cross section, which are due to thermal tension developed during high-speed drawing between adjacent holes. As the speed increases, the number of cracks at a given area also increases.

From Fig. 2, we found the average values of hole diameters d and adjacent hole spacings Λ of three HOFs and determined the corresponding fiber parameters for 0.633-, 1.33-, and 1.55-μm wavelengths. The measurement results are summarized in Table 1[13]. The diameters of outer layer of holes in three HOFs are measured about 82, 83, and 82 μm respectively, against the calculated theoretical value of 94 μm, which shows about 11% reasonable reduction in practical value.

It is observed that when the drawing speed increases, the holes spacings lower down in three fibers. By increase of drawing speed from 100 to 120 m/min, the average hole diameters of fibers No. 1 and 2 are reduced. A further increase in drawing speed has caused the average hole diameter of fiber No. 3 to increase. This is because at higher drawing speeds, the capillary tubes in the preform during the drawing process do not get enough time to collapse into smaller diameters.

To measure the NA and V_{eff} of the HOF, an experimental setup was arranged, as shown in Fig. 3(a), where a laser diode (LD) as a source and a photodiode (PD) as a photodetector have been used. The photodetector was mounted on an xyz positioner for a three-dimensional

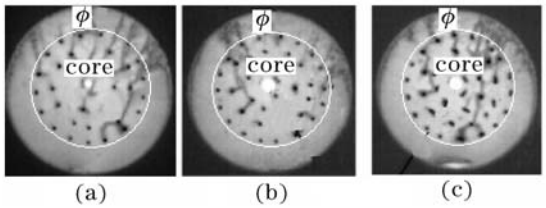

Fig. 2. Micrographs of drawn HOFs at different drawing speeds. (a) Fiber No. 1, v = 100 m/min, core diameter = 7.5 μm, ϕ = 82 μm; (b) fiber No. 2, v = 120 m/min, core diameter = 14.5 μm, ϕ = 83 μm; (c) fiber No. 3, v = 150 m/min, core diameter = 14 μm, ϕ = 82 μm.

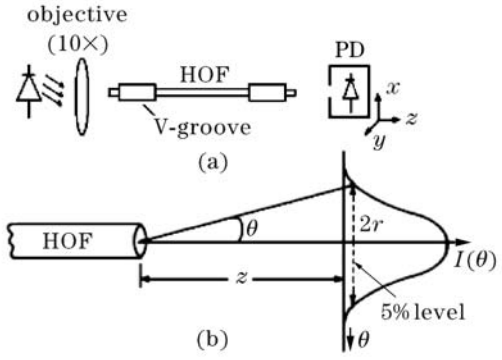

Fig. 3. (a) Experimental setup and (b) ideal far-field intensity distribution.

Table 1. Measured Parameters of Fabricated HOFs

Fiber	v	d	Λ	d/Λ	Λ/λ		NA		
No.	(m/min)	(μm)	(μm)		at 1.55 μm	at 1.33 μm	at 1.55 μm	at 1.33 μm	at 0.633 μm
1	100	3.6	15.66	0.23	10.16	11.77	0.1148	0.1075	0.0767
2	120	3.1	13.5	0.23	8.76	10.06	0.0596	0.0496	0.0293
3	150	3.4	13.2	0.26	8.55	9.90	0.2483	0.0937	0.0769

Table 2. Experimental Parameters of Refs. [15,16], and Present HOF for Comparison

Refs.	Fiber No.	Λ (μm)	d/Λ	A_{eff} (μm^2)			V_{eff}	
				at 1.55 μm	at 1.33 μm	at 0.633 μm	at 1.55 μm	at 0.633 μm
[15]	1	7.6	0.23	130	–	72	–	–
	2	9.7	0.23	215	–	100	–	–
	3	11.3	0.24	230	–	103	–	–
[16]	1	2.3	0.22	–	–	–	0.99	2.25
Present	1	15.66	0.23	58	49	22	4.66	7.63
HOFs	2	13.5	0.23	215	242	149	2.08	2.51

(3D) movement. The ideal far-field intensity pattern is shown in Fig. 3(b).

Based on far-field intensity distribution shown in Fig. 3(b), the field intensities were measured by help of the transversing detector at different wavelengths of 0.633, 1.33, and 1.55 μm. The field half-width is obtained with approximation, in which NA is calculated from $\text{NA} = \sin\theta \approx \tan\theta = r/z$, where the parameters θ, z, and r are as defined in Fig. 3(b). The effective normalized frequency V_{eff} is then determined by $V_{\text{eff}} = k_0\rho\text{NA}$. The effective mode area A_{eff} can be obtained as $A_{\text{eff}} = \pi(\text{MFD})^2/4$, where $\text{MFD} = 2w_0$ and $w_0 = \lambda/(\pi\tan\theta)$ is the far-field spot size[14].

By using our experimental HOF parameters given in Table 1, we have illustrated the effect of Λ/λ on effective normalized frequency V_{eff} in Fig. 4 with $d/\Lambda = 0.23$ at $\lambda = 1.55$ μm and compared the curves with theoretical and experimental results of Ref. [15], given in Table 2. Our results fairly tally with the results reported in Ref. [15]. The discrepancies between the theoretical and experimental results are due to the assumption of Gaussian mode and based on that, spot size measurements, which result in an error in calculation of NA and V_{eff} values. Another source of error could be due to difficulty in choosing an exact value of core radius when using effective index method for analysis of a HOF[15].

Figure 5 shows the NA measured experimentally with setup given in Fig. 3(a) with respect to wavelength at a measured value of $\Lambda = 13.5$ μm and $d/\Lambda = 0.23$. The trend of the NA changes almost follows the theoretical curve. Due to lower values of refractive index at higher wavelengths, the light in the cladding is confined less in the silica region and penetrates more into air holes, thus resulting in decrease of ERI of cladding. Therefore, the relative refractive index difference between core and

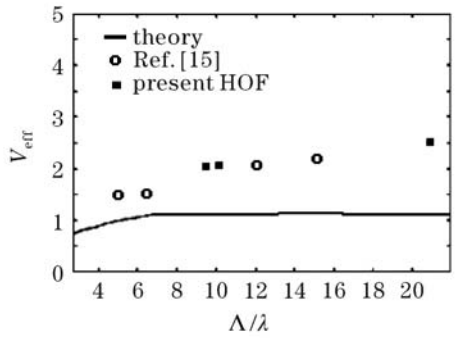

Fig. 4. Effective normalized frequency versus Λ/λ of the HOF with $d/\Lambda = 0.23$ at $\lambda = 1.55$ μm compared with Ref. [15].

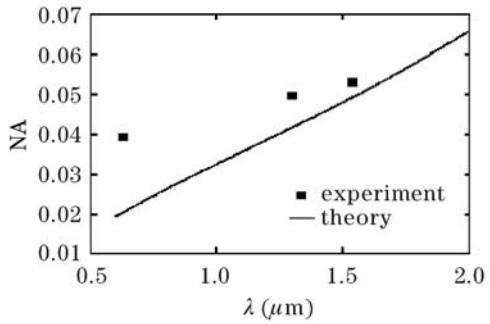

Fig. 5. NA versus wavelength λ at $\Lambda = 13.5$ μm and $d/\Lambda = 0.23$.

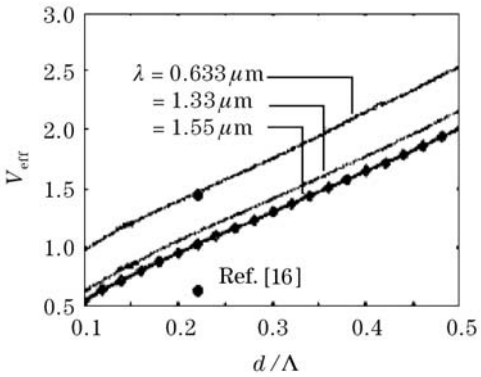

Fig. 6. Effective normalized frequency versus d/Λ of the HOF compared with Ref. [16] at $\lambda = 0.633$, 1.33, and 1.55 μm.

cladding increases, causing the NA to increase with increase in wavelength[10].

Since at lower wavelengths the confinement of light within the core of the HOF is less, the assumed Gaussian mode gets distorted. Therefore, with the same reasoning as in Fig. 4, the difference between theoretical and experimental values of NA in Fig. 5, may result from an erroneous measurement of spot size, on which the NA is dependent.

In Fig. 6, we have shown the variation of effective normalized frequency in terms of air filling coefficient d/Λ, using Eq. (6) with our experimental values at $\lambda = 0.633$, 1.33, and 1.55 μm. The curve is compared with the experimental results reported in Ref. [16], as given in Table 2. It shows that at a given Λ, the value of V_{eff} increases with increase in d/Λ. This increase is due to increase of NA which is the result of refractive index reduction in the cladding regions. In Ref. [16], the radius of the core is assumed Λ and in our analysis we have taken the radius to be $\rho = 0.64\Lambda$. Therefore, in comparison of

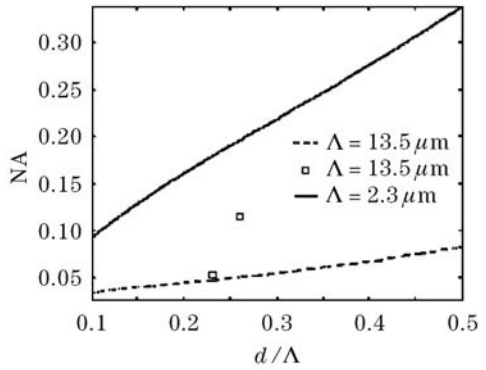

Fig. 7. NA versus d/Λ at $\lambda = 1.55$ μm for $\Lambda = 13.5$ and 2.3 μm. The dotted and solid curves show the theoretical NA variations.

our result with Ref. [16], a multiplying factor of 0.64 has been considered.

We have illustrated, in Fig. 7, the dependence of NA of fabricated HOFs as a function of d/Λ at $\lambda = 1.55$ μm for two measured values of $\Lambda = 13.5$ and 2.3 μm. By increasing the hole spacing Λ, the value of NA decreases, either, although the ratio d/Λ remains constant. This is logical because the percentage of air filling with respect to silica remains unchanged. In this case, the value of NA or the refractive index of cladding should not change since in ERI method, we have taken average values of refractive indices of air and silica as effective index value of the cladding.

A physical concept should be noted. That is, with increase in hole spacing, the waves with wavelengths less than 2 μm will less penetrate into air holes and are confined in the silica region of the cladding, thus increasing the refractive index of the cladding with respect to refractive index of core and hence resulting in reduction of NA of the fiber.

For the measured value of $d/\Lambda = 0.23$, we have shown NA of the fabricated HOF (fiber No. 2 in Table 1) with respect to Λ at $\lambda = 1.55$ μm and compared our results with theoretical prediction and Refs. [15,16] given in Table 2, as illustrated in Fig. 8. We observe that when hole spacing Λ increases, the value of NA lowers down, accordingly, justifying the statement given for Fig. 7.

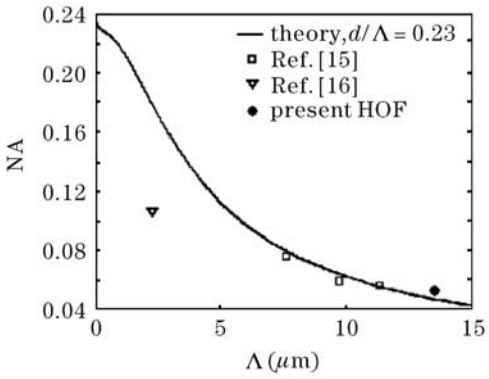

Fig. 8. NA of fabricated HOF versus Λ at $\lambda = 1.55$ μm with $d/\Lambda = 0.23$ compared with Refs. [15,16] and theoretical prediction.

In conclusion, the evaluation of transmission parameters of fabricated holey fibers drawn at high speeds is presented. The prepared preform was drawn at high speeds of 100, 120, and 150 m/min. The analyses of measurements of the NA and effective normalized frequency based on refractive index method are reported.

Although the fabricated HOFs did not have good quality in terms of hole regularity due to high speed drawing process, they have shown some reasonable characteristic parameters to be looked upon for more investigation on their production improvement at high speed fabrication.

The authors acknowledge the support of Iran Telecom Research Center for this work. F. E. Seraji's e-mail address is feseraji@itrc.ac.ir.

References

1. K. Ohsono, T. Nishio, Y. Bing, T. Shirosawa, and T. Sukegawa, Hitachi Cable Review **22,** 1 (2003).
2. T. M. Monro, P. J. Bennett, N. G. R. Broderick, and D. J. Richardson, Opt. Lett. **25,** 206 (2000).
3. J. C. Knight, T. A. Birks, P. St. Russel, and D. M. Atkin, Opt. Lett. **21,** 1547 (1996).
4. T. A. Birks, J. C. Knight, and P. St. J. Russel, Opt. Lett. **22,** 961 (1997).
5. T. M. Monro, D. J. Richardson, N. G. R. Broderick, and P. J. Bennett, J. Lightwave Technol. **17,** 1093 (1999).
6. F. E. Seraji, M. Rashidi, and V. Khasheie, Chin. Opt. Lett. **4,** 442 (2006).
7. K. Saitoh, Y. Tsuchida, and M. Koshiba, Opt. Lett. **30,** 1779 (2005).
8. J. B. Eom, K. W. Park, T.-J. Eom, Y. Chung, W.-T. Han, U.-C. Peak, and B. H. Lee, in *Proceedings of OECC2001* PDP2.05 (2001).
9. D. Kominsky, G. Pickrell, and R. Stolen, Opt. Lett. **28,** 1409 (2003).
10. S. K. Varshney, M. P. Singh, and R. K. Sinha, J. Opt. Commun. **24,** 192 (2003).
11. S. K. Varshney and R. K. Sinha, J. Microwaves and Optoelectron. **2,** 32 (2002).
12. F. E. Seraji, A. R. Hassani, N. Granpayeh, M. S. Zabihi, A. R. Bahrampour, and H. Amiri, in *Proceedings of 10th Photon. Conf. Iran* (2004).
13. M. Rashidi and F. E. Seraji, in *Proceedings of 12th Opt. Photon. Conf. Iran* (2006).
14. N. A. Mortensen, J. R. Folken, P. M. W. Skovgaard, and J. Broeng, IEEE Photon. Technol. Lett. **14,** 1094 (2002).
15. J. C. Baggett, T. M. Monro, K. Furusawa, V. Finazzi, and D. J. Richardson, Opt. Commun. **227,** 317 (2003).
16. J. C. Knight, T. A. Birks, P. St. J. Russel, and J. P. de Sandro, J. Opt. Soc. Am. A **15,** 748 (1998).